Acta Biomaterialia 90 (2019) 217–224

Contents lists available at ScienceDirect

Acta Biomaterialia

journal homepage: www.elsevier.com/locate/actabiomat

Full length article

Role of mechanical flow for actin network organization

Byungjun Kang [a], Seunghan Jo [a], Jonghyeok Baek [a], Fumihiko Nakamura [b], Wonmuk Hwang [c,d], Hyungsuk Lee [a,*]

[a] School of Mechanical Engineering, Yonsei University, Seoul 03722, Republic of Korea
[b] School of Pharmaceutical Science and Technology, Health Sciences Platform, Tianjin University, Tianjin 300072, China
[c] Departments of Biomedical Engineering, Materials Science & Engineering, and Physics & Astronomy, Texas A&M University, College Station, TX 77843, USA
[d] School of Computational Sciences, Korea Institute for Advanced Study, Seoul 02455, Republic of Korea

ARTICLE INFO

Article history:
Received 27 September 2018
Received in revised form 28 February 2019
Accepted 26 March 2019
Available online 27 March 2019

Keywords:
Actin
Cytoskeleton
Mechanical flow
Bundling
Actin binding protein

ABSTRACT

The major cytoskeletal protein actin forms complex networks to provide structural support and perform vital functions in cells. *In vitro* studies have revealed that the structure of the higher-order actin network is determined primarily by the type of actin binding protein (ABP). By comparison, there are far fewer studies about the role of the mechanical environment for the organization of the actin network. In particular, the duration over which cells reorganize their shape in response to functional demands is relatively short compared to the *in vitro* protein polymerization time, suggesting that such changes can influence the actin network formation. We hypothesize that mechanical flows in the cytoplasm generated by exogenous and endogenous stimulation play a key role in the spatiotemporal regulation of the actin architecture. To mimic cytoplasmic streaming, we generated a circulating flow using surface acoustic wave in a microfluidic channel and investigated its effect on the formation of networks by actin and ABPs. We found that the mechanical flow affected the orientation and thickness of actin bundles, depending on the type and concentration of ABPs. Our computational model shows that the extent of alignment and thickness of actin bundle are determined by the balance between flow-induced drag forces and the tendency of ABPs to crosslink actin filaments at given angles. These results suggest that local intracellular flows can affect the assembly dynamics and morphology of the actin cytoskeleton.

Statement of Significance

Spatiotemporal regulation of actin cytoskeleton structure is essential in many cellular functions. It has been shown that mechanical cues including an applied force and geometric boundary can alter the structural characteristics of actin network. However, even though the cytoplasm accounts for a large portion of the cell volume, the effect of the cytoplasmic streaming flow produced during cell dynamics on actin network organization has not been reported. In this study, we demonstrated that the mechanical flow exerted during actin network organization play an important role in determining the orientation and dimension of actin bundle network. Our result will be beneficial in understanding the mechanism of the actin network reorganization occurred during physiological and pathological processes.

1. Introduction

As one of the most abundant proteins in eukaryotic cells, the actin provides cells with mechanical integrity and carries out multifarious functions. Monomeric actins polymerize into filaments and further organize into higher-order structures with diverse morphologies [1]. Actin filaments anchored to the plasma membrane form the underlying cortex [2]. Bundles of F-actin (filamentous actin) of varying thicknesses are observed in stress fibers, filopodia, microvilli [3], and lamellipodia [4]. F-actin and myosin-II assemble into a contractile ring that carries out cytokinesis [5].

Organization of the actin cytoskeleton is primarily mediated by actin binding proteins (ABPs) [3,6–10]. With size ranging from 5 kDa to 3816 kDa, each ABP can confer specific structural characteristics to the network [6,11,12]. Yet, there must be additional factors. For example, deterioration of the morphology of microvilli is

* Corresponding author.
E-mail address: hyungsuk@yonsei.ac.kr (H. Lee).

https://doi.org/10.1016/j.actbio.2019.03.054
1742-7061/

not significant in ABP villin-knockout mice [13]. Similarly, actin stress fibers have been observed even after knockdown of the actin-bundling ABP, α-actinin [14]. These indicate that additional factors may play a role in regulating the actin cytoskeleton. Although physical constraints, such as the nucleation site of actin [15] and confinement of the actin network [16], and chemical polymerization conditions [17,18] were found to be important, mechanisms by which cells rapidly modulate the cytoskeletal architectures have yet to be elucidated [15,19].

Recent studies suggest that exogenous and endogenous mechanical stimuli can spatio-temporally regulate the structure of the actin network. For example, shear stress leads to stress-softening [20] or cyclic hardening [21]. Mechanical force generated by myosin motors causes local aggregation of actin filaments, buckling, and alignment of the actin network [22–26]. It has also been suggested that the cytoplasm acts like a poroelastic material [27] through which intracellular fluid can flow. Intracellular flow arises from a number of sources, such as cell migration [28,29] and cytokinesis [30] and reaches up to 100 μm/s [31]. Intracellular flow also occurs via stress relaxation under mechanical and chemical deformation of cells [32]. It can lead to protein conformational changes [33] and can regulate the kinetics and dynamics of actin [34,35]. Flow-induced shear stress also affects the affinity of ABPs to actin [36]. These findings suggest that intracellular flow can influence the organization of the actin cytoskeleton, which, to our knowledge, has not been investigated.

To systemically study the role of mechanical flow, we use reconstituted actin networks containing either of two representative ABPs: α-actinin, which tends to generate actin bundles [37], and filamin, which crosslinks actin filaments at an angle and tends to generate a meshwork-like structure [38]. As a proxy of intracellular flow, a microfluidic circulation was generated by employing the surface acoustic wave (SAW) technique [39]. We demonstrate that the actin networks formed with α-actinin and filamin respond differently to flow in terms of the network structure and degree of bundling. For α–actinin/actin, flow causes bundles to form and align more rapidly while the bundle thickness remains similar to the case without flow. In contrast, flow promotes thickening of the bundles in the filamin/actin system depending on their relative concentrations. We developed a computational model that captures the essential aspects of the experiments, where distinct crosslinking properties and geometries of two ABPs – α-actinin and filamin – modulate the effect of flow on the organization of the actin network. Present results suggest that intracellular flow can play a significant physical role in shaping the architecture of actin networks.

2. Materials and Methods

2.1. Fabrication of the SAW device

To generate SAW, interdigital transducers (IDTs) with a thickness of 100 nm were fabricated via photolithography on a 128° XY lithium niobate ($LiNbO_3$) piezoelectric substrate. The IDTs had 35-finger pairs, each with a length of 1.5 mm and a gap width of 70 μm. This design produced SAW with 280-μm wavelength. The center frequency of the SAW device was near 14 MHz, as measured by a network analyzer (8753C, Hewlett Packard, Palo Alto, CA, USA).

2.2. Flow generation in a microchamber using SAW

A microchamber with dimensions of $2 \times 18 \times 0.2$ mm (width × length × height) was prepared by attaching two strips of double-sided tape in parallel on a 24×40 mm coverglass. The top of the microchamber was covered with an 18×18 mm coverglass. The microchamber was then placed on polydimethylsiloxane spacers with a thickness of 100 μm, which were attached to a piezoelectric substrate in the SAW device. The coupling liquid (deionized water) was injected into the 100-μm space between the microchamber and the SAW substrate. A radio frequency (RF) signal applied to the IDTs was generated at 14 MHz using an RF signal generator (N5181A, Agilent Tech, Santa Clara, USA) and amplified by a power amplifier (100A250A, Amplifier Research, Souderton, PA, USA). The SAW generated on the piezoelectric substrate was transferred into the protein solution in the microchamber after passing through the coupling liquid and the coverglass. The transferred energy induced a pressure field and acoustic streaming field in the protein solution [40].

2.3. Flow speed characterization

To characterize the SAW-induced flow speed, we used a particle tracking method with microbeads that were 2 μm in diameter (Fluospheres® Fluorescent Microspheres, Molecular Probes, Eugene, OR, USA). Microbeads were diluted in the actin solution without the polymerization buffer at 0.001% (w/v) to ensure that individual beads were distinguishable. Movements of microbeads under flow with different input voltages were captured using an upright metallurgical microscope (BX60MF5, Olympus, Tokyo, Japan) equipped with a 5× objective and a CMOS camera (DFK 61AUC02, ImagingSource, Taipei, Taiwan). Movies were analyzed using MATLAB R2017a software (Mathworks, Natick, MA, USA).

2.4. Reconstituted F-actin networks

Lyophilized actin monomers and α-actinin, both purified from rabbit skeletal muscle, were purchased from Cytoskeleton, Inc, Denver, CO, USA. Recombinant filamin-A was purified from Sf9 cell lysates as previously described [41]. Actin monomer stocks were diluted in general actin buffer (5 mM Tris-HCl, 0.2 mM $CaCl_2$, 0.01% (w/v) NaN_3, 0.2 mM ATP, pH 8.0) and incubated on ice for 2 h. ABPs were also diluted in the general actin buffer. The ABP solution was mixed with Alexa Fluor 532 Phalloidin (Invitrogen, Carlsbad, CA, USA), which fluorescently labels actin filaments. The molar concentration of Phalloidin was one-tenth of that of actin monomers to minimize the Phalloidin-induced perturbation of actin networks. The actin polymerization buffer (50 mM Tris-HCl, 500 mM KCl, 2 mM $MgCl_2$, 2 mM $CaCl_2$, 5 mM ATP, 0.01% (w/v) NaN_3, pH 7.5) was used to dilute the phalloidin-labeled ABP solution by 10-fold. Finally, the G-actin solution was mixed with the prepared solution to initiate polymerization. The final concentrations were 5 and 10 μM for G-actin, 0.5, 1, 2, 2.5 and 5 μM for α-actinin and 0.1, 0.25, 0.5 and 1 μM for filamin. The concentrations of actin and ABPs were similar to those found in cells [42–46]. The volume of the actin polymerization buffer was one-tenth of the volume of the mixed solution. The mixed solution was gently pipetted and transferred into the chamber. The microchamber was sealed with vacuum grease to prevent sample drying. Actin polymerization occurs in the presence of mechanical flow applied by the SAW. To see if the staining using phalloidin affects our experimental results, we performed an experiment using a fluorescent dye-conjugated actin. The dye-conjugated actin network exhibited the similar actin alignment by flow compared to the actin networks obtained using phalloidin (Fig. S1).

2.5. Optical imaging and image processing

A laser scanning confocal microscope (LSM 510 META, Carl Zeiss, Oberkochen, Baden-Württemberg, Germany) with a 20× objective and a 40× water immersion objective was used to acquire fluorescent images of the actin networks. It was difficult to obtain in situ images of actin network formation due to the com-

plexity of the SAW device and limited scanning rate of the confocal microscope. Instead, we obtained the image of actin network after polymerization was completed. All images were taken after 1 h of polymerization in the center of the chamber to minimize boundary effects. A total of 51 image stacks separated vertically by 200 nm were projected to visualize the entire bundle networks. The degree of alignment of the actin bundles was quantified by applying a 2-dimensional Fast Fourier Transform (2D FFT) that has been used to analyze the alignment of collagen fibers [47]. First, the images were converted into grayscale images, and 2D FFT was applied using the NIH Image J version 1.51t [48]. Using the 'Oval profile' plugin [49] in ImageJ, the sum of pixel intensities along a straight line from the center of the FFT image at a given orientation from 0° to 180° was obtained. The peak angle of the intensity distribution was re-centered to 0°, and the distribution was normalized to yield a unit area. The area δ of the normalized intensity distribution within ±20 degrees around the peak was calculated. For a random uniform distribution, area δ was 40/180 = 0.22. The alignment index (AI) was defined as the ratio δ/0.22. An AI value of 1 indicates an isotropic distribution of actin bundles, and as actin bundles are increasingly aligned in one direction, the AI approaches the maximum value of 4.5 (=1/0.22).

2.6. Bundle thickness measurement

Actin structures were attached to the coverslip surface using the method reported by Nakao et al. [50]. After washing the sample with DI water 3 times, we used a 3D laser scanning microscope (VK-X100, Keyence, Neu-Isenbuerg, Germany) to acquire surface profile images. The thickness of the actin bundle was estimated from the height difference between a given peak and the average of the two valley points around it. As a test, we estimated the thickness of a single actin filament and compared it with that measured by TEM (Transmission Electron Microscopy).

2.7. Computational model of actin network formation under mechanical flow

Using a kinetic model developed to consider actin nucleation, polymerization, and depolymerization by Falzone et al. [51], length of actin filament varies with time as followed:

$$L(t) = \begin{cases} (4/50 \times t)\ \mu\text{m} & (t \le 50s) \\ 4\ \mu\text{m} & (t > 50s) \end{cases}$$

where L is length of actin filament and t is time in second.

An actin filament was modeled as a rigid rod [26,52]. Actin and ABP were randomly placed in a finite two-dimensional space having periodic boundary condition [52]. We considered two types of ABPs: bundling ABP α-actinin and crosslinking ABP filamin.

ABPs bind to and detach from the intersection between two actin filaments or bundles with binding and unbinding probabilities of $p_b = k_{on}C_{ABP}\Delta t$ and $p_{unb} = k_{off}\Delta t$, respectively [53], with the association (dissociation) rate constant k_{on} (k_{off}), ABP concentration C_{ABP}, and simulation time step Δt. If both the angle between two filaments and their center-to-center distance are smaller than the threshold values, the filaments form a bundle with probability p_b. At bundling, two actin filaments become an actin bundle with the thickness equal to the sum of the thickness of the two parent filaments. Dissociation of actin bundle into single filaments is not allowed because it is highly unlikely for ABPs to unbind simultaneously from the bundle.

ABP bound at an intersection acts as a torsional spring which generates a torque $\mathbf{T}_{\boldsymbol{cross}} = -k_T\left(\theta^{ij} - \theta_{eq}\right)\widehat{\mathbf{e}_z}$ (k_T: torsional stiffness, θ_{eq}: equilibrium angle of the ABP, θ^{ij}: angle between two filaments i and j, and $\widehat{\mathbf{e}_z}$: unit vector perpendicular to the 2D simulation domain).

An actin filament of length L and thickness H in a fluid with viscosity μ and temperature T undergoes translational and rotational Brownian motion with diffusion coefficients of $D_\parallel = k_BT/\xi_\parallel$, $D_\perp = k_BT/\xi_\perp$ and $D_r = k_BT/\xi_r$ for longitudinal and transverse translation, and rotation of the filaments (k_B: Boltzmann's constant), respectively [54]. The drag coefficients for longitudinal, transverse, and rotational motion are $\xi_\parallel = 2\pi\mu L/(\ln(L/H) - 0.20)$, $\xi_\perp = 4\pi\mu L/(\ln(L/H) + 0.84)$, and $\xi_r = (\pi\mu/3) \times \left(L^3/(\ln(L/H) - 0.66)\right)$, respectively [55]. The corresponding mean square displacement or angle is $2D_\parallel\Delta t$, $4D_\perp\Delta t$, and $4D_r\Delta t$ for the longitudinal, transverse translation and rotation, respectively [56]. Actin filaments are set to move (rotate) with a displacement (angle) equal to the square root of the mean square displacement (angle) times the random probability between −1 and 1.

Flow causes a longitudinal and transverse drag force $\mathbf{F}_{\boldsymbol{drag},\parallel} = \xi_\parallel(\mathbf{v}_{\boldsymbol{flow},\parallel} - \mathbf{v}_{\boldsymbol{filament},\parallel})$ and $\mathbf{F}_{\boldsymbol{drag},\perp} = \xi_\perp(\mathbf{v}_{\boldsymbol{flow},\perp} - \mathbf{v}_{\boldsymbol{filament},\perp})$ ($\mathbf{v}_{\boldsymbol{flow},\parallel}$, $\mathbf{v}_{\boldsymbol{flow},\perp}$, $\mathbf{v}_{\boldsymbol{filament},\parallel}$, and $\mathbf{v}_{\boldsymbol{filament},\perp}$: longitudinal and transverse velocity of flow and filament, as obtained by decomposing the velocity into respective directions relative to the orientation of the filament at each simulation step). In the overdamping limit, we neglected the inertia effect [57,58] so that the velocity of the actin filament is the same as the flow velocity.

A single actin filament under a simple shear flow rotates with an angular speed $\dot{\theta} = |\mathbf{v}_{\boldsymbol{flow}}|/h \times \sin^2(\theta - \theta_{flow})$ [35] (θ_{flow}: direction of flow, θ: direction of the filament, and h: half of the channel height). When actin filaments i and j are crosslinked, the drag force generates a torque $\mathbf{T}_{\boldsymbol{flow}} = (\boldsymbol{r}^{ij} \times \mathbf{F}_{\boldsymbol{drag}})$ at the intersection where $\mathbf{r}^{ij}$ is the vector from the center of the filament i to the intersection of filament i and j. Torques on the actin filament should be balanced as $-\xi_r\dot{\theta} + \mathbf{T}_{\boldsymbol{cross}} + \mathbf{T}_{\boldsymbol{flow}} = 0$ [26,59]. The location and angle of filaments at time $t + \Delta t$ were calculated by using Euler integration [60–62]. Parameters utilized in the simulation are summarized in Table S1.

2.8. Statistical analysis

Data are presented as the mean ± standard deviation. Statistical significance was evaluated using unpaired Student's t-test.

3. Results

3.1. Effect of mechanical flow on actin networks architectures

The speed of mechanical flow generated by SAW (Fig. 1A) was in the range of 0 ~ 25 μm/s at 5 μM actin, which is comparable to the speed of cytoplasmic streaming [31,63–66] (Fig. 1B). We polymerized actin network subject to mechanical flow for an hour

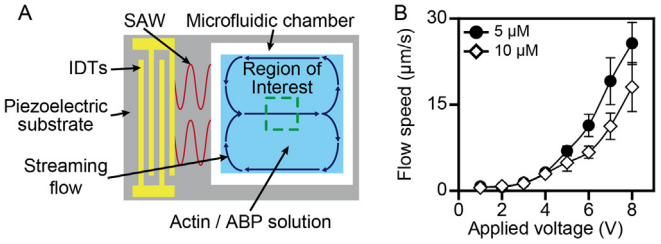

Fig. 1. Generation of the flow mimicking cytoplasmic streaming in a confined chamber. (A) Experimental scheme. (B) Flow velocity of actin solution at various actin concentrations in the center region of microfluidic chamber at different input voltages. N = 9 for each.

and visualized using confocal microscopy. Images were taken at the center region of the chamber where flow is unidirectional. In the absence of flow, α-actinin/actin (1 μM α-actinin and 5 μM actin) formed a homogeneous network with relatively short actin bundles (Fig. 2A). Flow caused α-actinin/actin bundles to align. The degree of alignment increased with flow (Fig. 2A). By contrast, flow-induced alignment was less prominent for the filamin/actin network (0.5 μM filamin and 5 μM actin), and broken networks of actin bundles formed instead (Fig. 2B). Higher susceptibility of the α-actinin/actin network to align under flow could also be seen via quantification using the alignment index (AI) [47] (Fig. 2C).

We investigated the effect of ABP concentration on the actin network alignment (Fig. 3A). For α-actinin/actin without flow, AI increased slightly with increasing α-actinin concentration, which is likely due to the formation of elongated clusters. With flow, AI was higher at α-actinin concentrations of 1 μM and above (Fig. 3B). Comparable levels of AI at 1 and 2.5 μM α-actinin may be due to extensive crosslinking that leads to rapid formation of actin networks and impedes rotation of individual bundles. For the filamin/actin system without flow, some actin bundles were observed at 0.25 μM filamin (Fig. 4A). Although thicker bundles formed at higher filamin concentrations, the network was less uniform compared to the α-actinin/actin network. Unlike the α-actinin/actin case, flow did not increase the level of alignment, as revealed by the AI (Fig. 4B). The filamin/actin network was also non-uniform and disconnected, similar to the case without flow. We also investigated the effect of flow on the alignment at a higher actin concentration, 10 μM, while varying the concentration of α-actinin (Fig. S2). Flow enhanced alignment at low and intermediate α-actinin concentrations. But when both actin and ABP concentrations were high, aggregates of thick bundles formed independent of flow, which is again consistent with the rapid formation of an immobile network. These suggest that the effect of flow depends on the kinetics of actin polymerization, ABP crosslinking, and actin filament bundling.

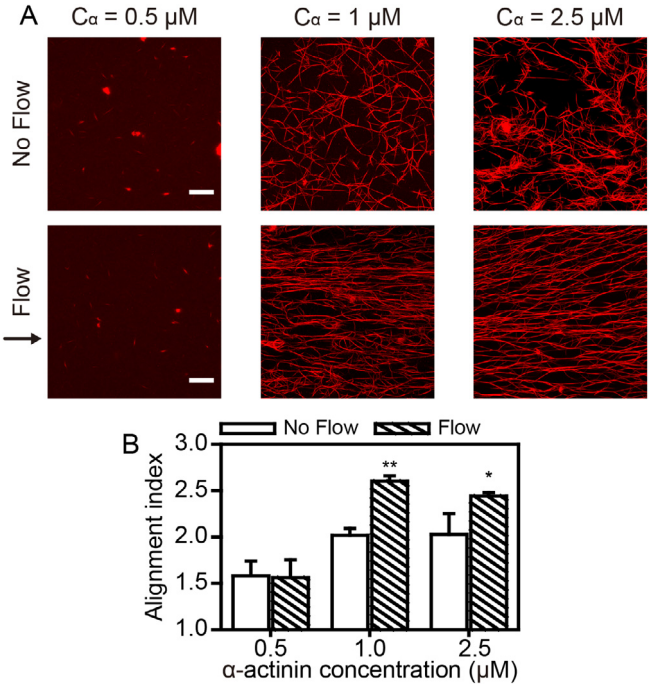

Fig. 3. Dependence of the α-actinin/actin network architecture on the ABP concentration with and without mechanical flow. (A) Confocal images of 5 μM actin and various concentrations of α-actinin (C_α). Flow speed for bottom rows is 25 μm/s. Scale bars: 30 μm. (B) AI corresponding to experiments in (A). N = 3 for each. Error bars represent one standard deviation. (Student's t-test, $^*p < 0.1$, $^{**}p < 0.01$ versus No Flow group).

3.2. Effect of mechanical flow on the bundle thickness within actin networks

We further studied the effect of flow on the bundle thickness. To assess the resolution of our technique, we first measured the thickness of a single actin filament, which was 10.8 ± 3.0 nm (N = 48) similar to the estimate from TEM (Fig. 5A–D). We then compared the thickness of bundles formed at various flow speeds. Actin bundles formed with α-actinin at different flow speeds had similar height profiles (Fig. 5E–G). In contrast, networks formed with filamin had heights increasing with the flow speed (Fig. 5H–J). Quantitative analysis for bundles formed at various ABP concentrations at a given actin concentration found that the thickness increased with concentration independent of the presence of flow for α-actinin (Fig. 6A), similar to the thickening of bundles with the α-actinin concentration in the absence of flow [67–69]. For filamin, the bundle thickness with flow was estimated to be higher at filamin concentrations smaller than 0.1 times the concentration C_a below which no bundle was observed with no flow (Fig. 6B). It indicates that an applied flow reduces the 'critical concentration' of filamin above which actin bundles rather than orthogonal networks form [38]. Taken together, the flow facilitates alignment without affecting the bundling for α-actinin while it promotes bundling for filamin. Our result is physically intuitive considering the characteristics of these ABPs. Since α-actinin bun-

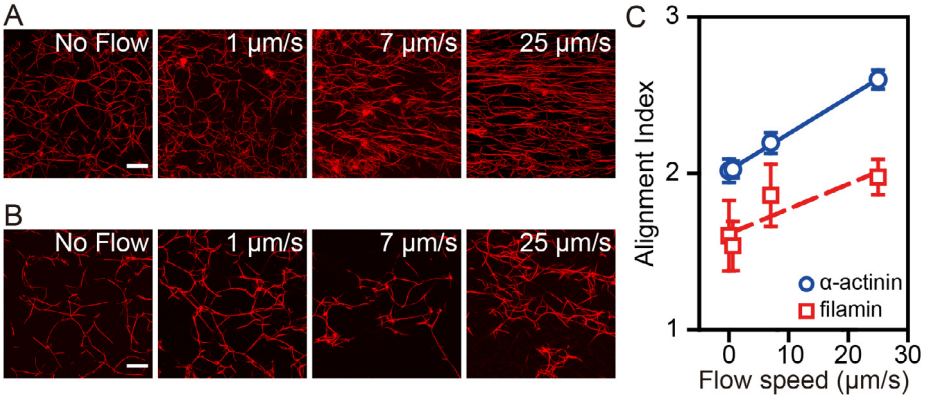

Fig. 2. Effect of mechanical flow on the architecture of crosslinked actin networks. (A, B) Confocal images (projections of 51 image stacks spanning 10 μm in height). (A) 1 μM α-actinin/5 μM actin and (B) 0.5 μM filamin/5 μM actin. A direction of flow is to the right and the flow speed is marked in each panel. Scale bars: 30 μm. (C) AI for 1 μM α-actinin/5 μM actin and 0.5 μM filamin/5 μM actin, versus flow speeds. N = 3 for each. Error bars represent one standard deviation.

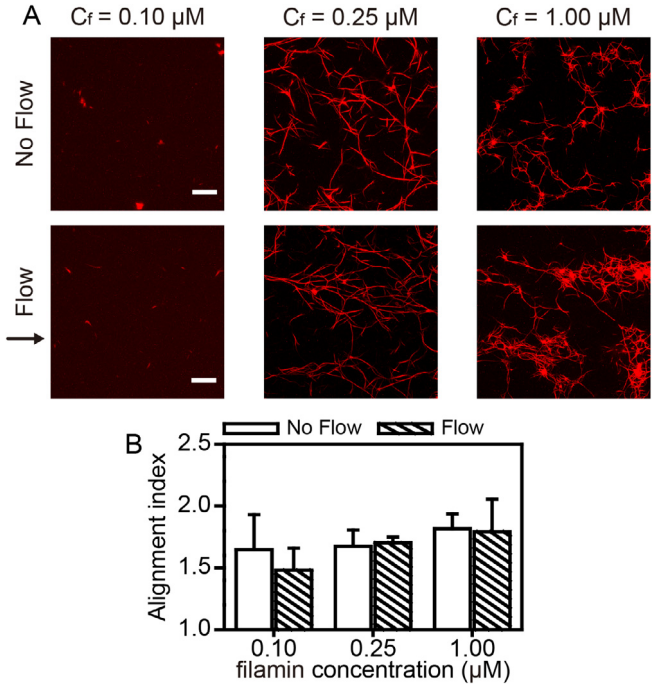

Fig. 4. Dependence of the filamin/actin network architecture on the ABP concentration with and without mechanical flow. (A) Confocal images of 5 μM actin and various concentrations of filamin (C_f). Flow speed for bottom rows is 25 μm/s. Scale bars: 30 μm. (B) AI corresponding to experiments in (A). N = 3 for each. Error bars represent one standard deviation.

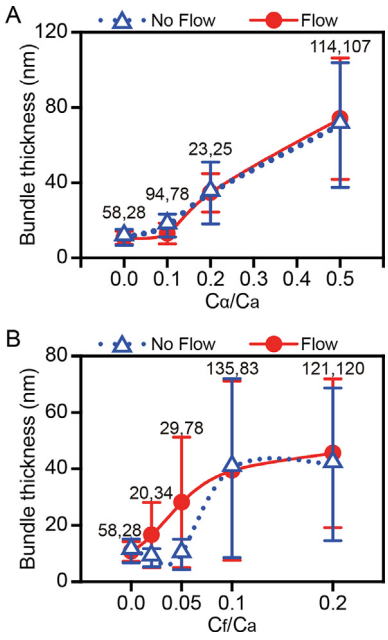

Fig. 6. Thickness of actin bundles at 5 μM organized with various molar ratios of ABP to actin with and without mechanical flow for (A) α-actinin (C_α/C_a) and (B) filamin (C_f/C_a). C_α, C_f, and C_a are the concentration of α-actinin, filamin, and actin, respectively. Flow speed was 25 μm/s. Numbers above data points represent sample sizes for cases without and with the flow. Error bars represent one standard deviation.

dles the actin filaments, the primary effect of flow is to promote alignment. On the other hand, since filamin tends to make orthogonal crosslinks, flow can enhance bundling.

3.3. Computational model of actin network formation under mechanical flow

To semi-quantitatively elucidate the effect of the applied flow on the organization of the actin network, we developed a stochastic simulation in 2-dimensions that incorporates minimal features of the ABP/actin system (see Methods). Our model assumes that ABPs bind at every intersection between filaments, and drive their angles to decrease/increase for the bundling/crosslinking ABP, respectively (Fig. 7A). Bundling between filaments occurs when they are nearly parallel, and the distance between the centers of the filaments is smaller than the size of an ABP, which is 30 nm and 110 nm for the bundling and crosslinking ABP, respectively. Upon formation of a bundle, it is treated as a single filament with an increased thickness.

Flow causes filaments to rotate and translate. Isolated filaments rotate about the center of mass, while crosslinked filaments rotate about the crosslinking points. For the bundling ABP, since it reaches mechanical equilibrium when filaments are parallel, flow-induced alignment helps with rapid bundling (Fig. 7B, left). In contrast, the crosslinking ABP's tendency to make filaments orthogonal to each other competes with flow-induced alignment. As a result, the flow hinders the formation of orthogonal crosslinks (Fig. 7B, right).

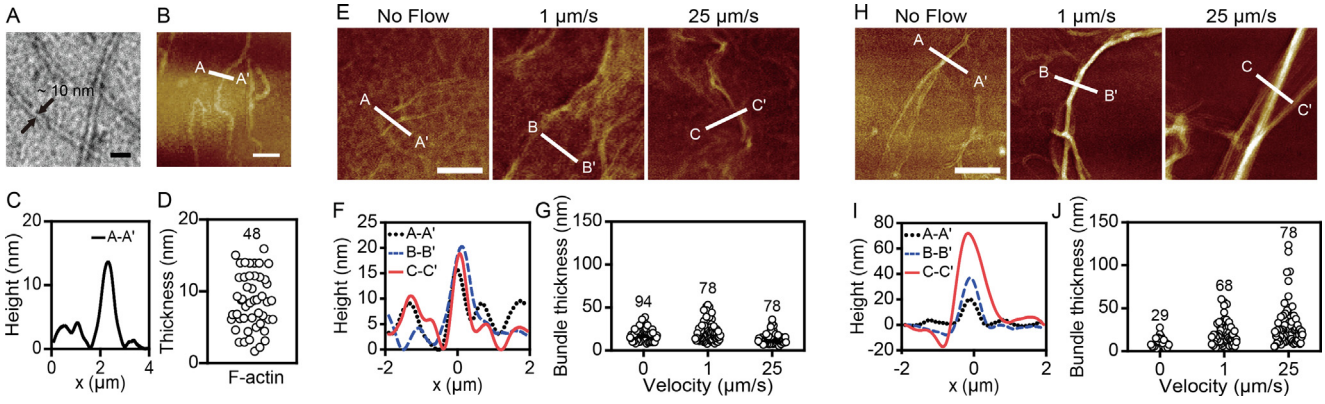

Fig. 5. Effect of mechanical flow on the thickness of actin bundle. (A) TEM image (scale bar: 30 nm) and (B) 3D laser microscopy image (scale bar: 5 μm) of single actin filaments. (C) Height distribution of the A-A' line in panel (B). (D) Scatter plot of the thickness of single actin filaments. 3D laser microscopy images (scale bars: 5 μm), height distributions of the lines in the 3D images, and scatter plot of the corresponding bundle thickness for 0.5 μM α-actinin/5 μM actin (E, F, G) and 0.25 μM filamin/5 μM actin (H, I, J) networks polymerized under various flow speeds. The number above data points represents sample size for each condition.

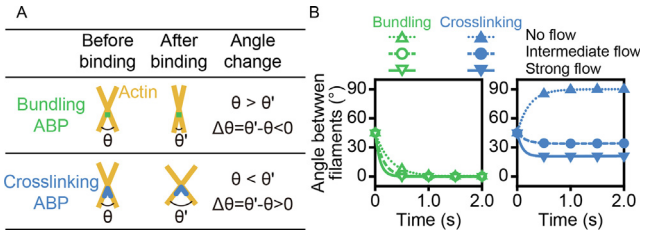

Fig. 7. Computer simulation of crosslinking of actin filaments by ABP. (A) Schematic description of the model. (B) The average angle between 4 μm filaments in simulations with bundling and crosslinking ABPs.

At the beginning of simulation, actin filaments grow in length until they reach the steady-state length, 4 μm. During the initial growth phase (before 10 s), actin filaments did not interact with each other because they were short. Crosslinking or bundling occurred mostly when actin filaments became long enough to contact each other (Fig. 8A).

In the absence of flow, the simulation system with the bundling ABP formed isotropically distributed filaments, whereas orthogonal networks formed in the case with crosslinking ABP (Fig. 8A). Flow resulted in the alignment of bundles for both types of ABPs. For the crosslinking ABP, flow-induced alignment occurred more slowly and less extensively compared to the bundling ABP (Fig. 8A). Time-dependent changes in AI confirmed faster and more extensive alignment for the case with the bundling ABP (Fig. 8B). In addition, we investigated how actin nucleation and ABP binding kinetics affect actin network organization subject to flow (Figs. S3 and S4). Our results found that those effects were not significant in terms of actin filament alignment, suggesting that the flow effect was more dominant in our given condition. Furthermore, flow reduces the probability of forming thick bundles in α-actinin/actin networks, since the alignment of small bundles make them spatially separated so that further bundling becomes difficult. In contrast, thicker bundles formed in filamin/actin networks when flow was applied (Fig. 8C). This is because crosslinking at a larger angle allows filaments over a greater area to be connected and bundled by flow. We also investigated the effect of ABP concentration on the formation of actin network subject to flow. For the bundling ABP, there was not a significant change in the flow-dependent formation of actin bundles (Fig. S5A). For crosslinking ABP, the flow did not promote actin filament bundling when the ABP concentration increased, as in our experiment (Fig. S5B).

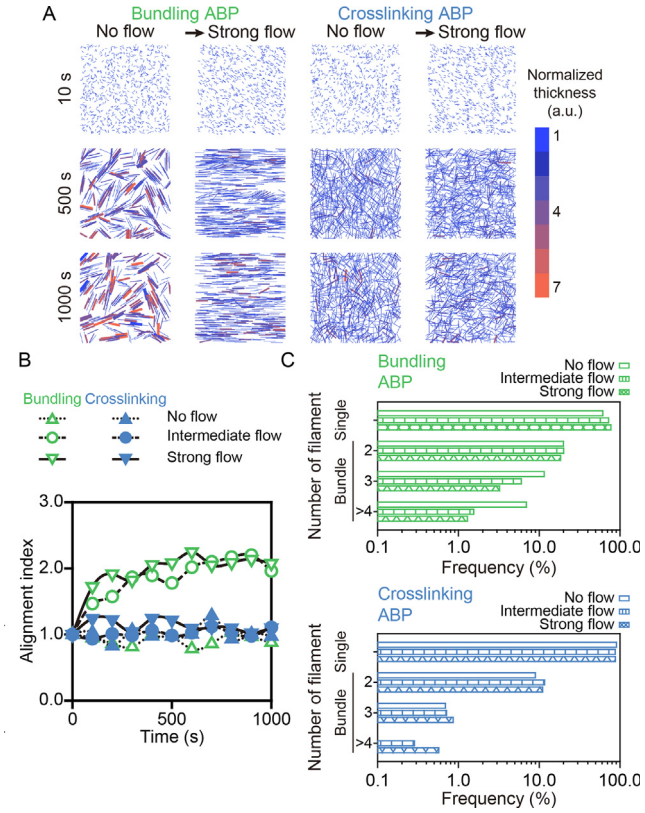

Fig. 8. Computer simulation of flow-induced bundling of actin filaments. (A) Time evolution of the networks crosslinked by bundling and crosslinking ABPs, with and without a strong flow. (B) AI versus the simulation time steps. (C) Distribution of the bundle thickness for the case with bundling and crosslinking ABPs. The molar ratios of ABP to actin for bundling ABP ($C_{bundling}/C_a$) and crosslinking ABP ($C_{crosslinking}/C_a$) were 0.2 and 0.1 for (B) and 0.1 and 0.05 for (C), respectively. $C_{bundling}$, $C_{crosslinking}$, and C_a are the concentration of bundling ABP, crosslinking ABP, and actin, respectively.

4. Discussion

Similar to our work *in vitro*, mechanical flow likely affects the organization of the actin cytoskeleton in cells. The critical flow speed at which an extensive alignment of actin network was observed is approximately 7 μm/s (Fig. 2C). In comparison, the cytoplasmic flow in animal cells *in vivo* is in the range of $0.1 \sim 1$ μm/s [28,70]. However, the viscosity of the cytoplasm is 10- to 300-fold higher than that of the aqueous solution in our *in vitro* experiments [58,71,72]. Drag force on actin due to cytoplasmic flow should thus be comparable to or even higher than that of our experiment. We estimate the shear stress in our microfluidic chamber as follows. Assuming that Poiseuille flow is established in the channel, the flow velocity exhibits a parabolic profile. Near the wall of the channel, actin filament would experience shear stress of 0.045 pN/μm^2 (Fig. S6A), which is indeed comparable to 0.01–6 pN/μm^2 as previously measured in cells [73]. To further study the effect of higher viscosity of the cytoplasm, we performed an experiment with a 70 kDa dextran added to the actin solution [74,75]. In this case, actin filaments were aligned at a lower speed (1 μm/s) (Fig. S7A). From the computational analysis, we also observed that the alignment index of actin network with bundling ABP is increased by the fluid viscosity at low flow speed (Fig. S7B).

Our computational model revealed the mechanism by which the applied flow influences actin bundling and network formation by regulating the orientation and ultimately cross-linking of actin filaments. But we also note certain limitations of our model in representing properties of actin and ABP. Since the bending rigidity of actin filament [11] is 10^{-26} Nm^2, the applied flow can cause not only rotational displacement but bending of long actin filament. The bending motion will assist encounter between filaments in the semi-dilute or concentrated conditions [76], which may accelerate the actin network formation. However, lengths of actin filaments in cells are under 1 μm [77,78], which is much smaller than their persistence length (17 μm) [79]. Persistence lengths of actin bundles will be even longer, and the tensile stress on the actin filament by the actomyosin machinery [8] can increase resistance to bending. Thus, treating actin filaments as rigid rods in our computational model is a reasonable first-hand approximation.

The interaction between actin and ABP, including dissociation constant and torsional stiffness, depends on applied force and loading rate [80,81]. A critical shear strain at which binding affinity of filamin to β-integrin or FilGAP (filamin A binding RhoGTPase-activating protein) was altered was 28% [82]. The maximum moment produced by flow on a single actin filament in our experimental condition is approximately 2.38×10^{-20} Nm (Fig. S6B),

which is enough to exert shear strain greater than the critical value. A single molecule assay showed that filamin/actin and α-actinin/actin complexes ruptured at the pulling force of 40–80 pN [36,83]. As stress on a crosslink in the actin network can be increased by its heterogeneous deformation [84] as well as the shear force applied to the actin filaments, rebinding or unfolding (Fig. S6C) of ABP can occur. Incorporation of these elements in simulation is a subject of future studies.

Another aspect is the complexity of the cytoplasmic flow. Due to viscoelastic properties [85], cells can undergo significant mechanical deformation by exogenous or endogenous mechanical forces. Transition between sol-like and gel-like states occurring in organelles lead to dynamic changes of local properties in cells [86]. Cytoplasm is also a non-Newtonian liquid where the viscosity changes with velocity [87]. Therefore, the magnitude and direction of the cytoplasmic flow are more complicated compared to the bi-directional pattern occurred in our experiment [29,65]. The complexity of the cytoplasmic flow may affect the role of flow on actin network formation. But within domains where the flow can be considered relatively uniform, the effects as revealed in the present study should hold.

Components of cells are also more complicated compared to those modeled in our study. The cytoplasm consists of many constituents including types of cytoskeleton filament, organelles, dissolved molecules and proteins. As for actin binding proteins, we investigated the effect of flow on the organization of actin bundles in the presence of α-actinin and filamin which prefer parallel bundling and orthogonal cross-linking of actin filaments, respectively. However, other types of ABPs are present in cells. Severing ABPs such as gelsolin and cofilin [88] make the length of actin filaments and the distance between intersections of actin network in cells shorter than those *in vitro* (Fig. S8) [8,77,89]. Motor proteins such as myosin produce contractile stress on actin filaments [1]. Arp2/3 complex is a branching ABP that forms a Y-shape crosslink rather than the X-shape as with filamin [90]. The cytoskeleton in a cell is surrounded by the cell membrane and ABP talin connects actin filaments to the transmembrane protein integrin [91]. Therefore, the effect of flow at the membrane boundary would be different compared to regions relatively far from the membrane. The present study elucidates a simplified scenario, which will help to understand how flow synergistically affects the organization and dynamics of actin networks by these ABPs.

5. Conclusion

The present work uses flow generated by surface acoustic wave in a confined chamber as a proxy of cytoplasmic streaming in the intracellular environment. Our results suggest that flow is an important regulator of the crosslinked actin network organization, where the effect of flow depends on the type and concentration of ABP. With the bundling ABP α-actinin, flow enhanced mainly alignment of the actin network, not bundle thickness. Converse behaviors were observed with the crosslinking ABP filamin, where flow promoted bundle formation without enhancing alignment, and it reduced the critical filamin concentration for bundling. Our computational model elucidates how the structural and crosslinking properties of ABPs modulate the effect of flow on the actin bundle network organization. Taken together, the cytoplasmic streaming can serve as a regulator for the cytoskeleton organization as well as facilitate intracellular transport.

Acknowledgements

The authors would like to thank Professor No-Cheol Park, Professor Won-Suk Ohm, and Professor Dae-Eun Kim for their cooperation in using the equipment. This work was supported by the National Research Foundation of Korea (NRF, South Korea) grants funded by the Korea Government (2018R1A2A3075287) and the Institute of Convergence Science (ICONS) at Yonsei University.

Appendix A. Supplementary data

Supplementary data to this article can be found online at https://doi.org/10.1016/j.actbio.2019.03.054.

References

[1] D.A. Fletcher, R.D. Mullins, Cell mechanics and the cytoskeleton, Nature 463 (2010) 485–492.
[2] G. Salbreux, G. Charras, E. Paluch, Actin cortex mechanics and cellular morphogenesis, Trends Cell Biol. 22 (2012) 536–545.
[3] J.R. Bartles, Parallel actin bundles and their multiple actin-bundling proteins, Curr. Opin. Cell Biol. 12 (2000) 72–78.
[4] P.K. Mattila, P. Lappalainen, Filopodia: molecular architecture and cellular functions, Nat. Rev. Mol. Cell Biol. 9 (2008) 446–454.
[5] K. Murthy, P. Wadsworth, Myosin-II-dependent localization and dynamics of f-actin during cytokinesis, Curr. Biol. 15 (2005) 724–731.
[6] O. Lieleg, M.M.A.E. Claessens, A.R. Bausch, Structure and dynamics of cross-linked actin networks, Soft Matter 6 (2010) 218–225.
[7] R.K. Meyer, U. Aebi, Bundling of actin filaments by alpha-actinin depends on its molecular length, J. Cell Biol. 110 (1990) 2013–2024.
[8] M.L. Gardel, F. Nakamura, J.H. Hartwig, J.C. Crocker, T.P. Stossel, D.A. Weitz, Prestressed F-actin networks cross-linked by hinged filamins replicate mechanical properties of cells, Proc. Natl. Acad. Sci. U.S.A. 103 (2006) 1762–1767.
[9] H.N. Higgs, T.D. Pollard, Regulation of actin filament network formation through ARP2/3 complex: activation by a diverse array of proteins, Annu. Rev. Biochem. 70 (2001) 649–676.
[10] D.H. Wachsstock, W.H. Schwartz, T.D. Pollard, Affinity of alpha-actinin for actin determines the structure and mechanical properties of actin filament gels, Biophys. J. 65 (1993) 205–214.
[11] H. Lee, Mechanical Properties of F-actin Network, Massachusetts Institute of Technology, 2009.
[12] Y. Hathout, R.L. Marathi, S. Rayavarapu, A. Zhang, K.J. Brown, H. Seol, H. Gordish-Dressman, S. Cirak, L. Bello, K. Nagaraju, Discovery of serum protein biomarkers in the mdx mouse model and cross-species comparison to Duchenne muscular dystrophy patients, Hum. Mol. Gen. 23 (2014) 6458–6469.
[13] E. Ferrary, M. Cohen-Tannoudji, G. Pehau-Arnaudet, A. Lapillonne, R. Athman, T. Ruiz, L. Boulouha, F. El Marjou, A. Doye, J.-J. Fontaine, In vivo, villin is required for Ca 2+-dependent F-Actin disruption in intestinal brush borders, J. Cell Biol. 146 (1999) 819–829.
[14] L. Lu, Y. Feng, W.J. Hucker, S.J. Oswald, G.D. Longmore, F.C.P. Yin, Actin stress fiber pre-extension in human aortic endothelial cells, Cell Motil. Cytoskeleton 65 (2008) 281–294.
[15] A.-C. Reymann, J.-L. Martiel, T. Cambier, L. Blanchoin, R. Boujemaa-Paterski, M. Théry, Nucleation geometry governs ordered actin networks structures, Nat. Mater. 9 (2010) 827–832.
[16] M.S. e Silva, J. Alvarado, J. Nguyen, N. Georgoulia, B.M. Mulder, G.H. Koenderink, Self-organized patterns of actin filaments in cell-sized confinement, Soft Matter 7 (2011) 10631–10641.
[17] K.M. Schmoller, S. Köhler, A.H. Crevenna, R. Wedlich-Söldner, A.R. Bausch, Modulation of cross-linked actin networks by pH, Soft Matter 8 (2012) 9685–9690.
[18] M. Tempel, G. Isenberg, E. Sackmann, Temperature-induced sol-gel transition and microgel formation in α-actinin cross-linked actin networks: a rheological study, Phys. Rev. E 54 (1996) 1802.
[19] H. Yamaguchi, J. Condeelis, Regulation of the actin cytoskeleton in cancer cell migration and invasion, Biochim. Biophys. Acta 1773 (2007) 642–652.
[20] O. Chaudhuri, S.H. Parekh, D.A. Fletcher, Reversible stress softening of actin networks, Nature 445 (2007) 295–298.
[21] K.M. Schmoller, P. Fernandez, R.C. Arevalo, D.L. Blair, A.R. Bausch, Cyclic hardening in bundled actin networks, Nat. Commun. 1 (2010) 134.
[22] M.S. e Silva, M. Depken, B. Stuhrmann, M. Korsten, F.C. MacKintosh, G.H. Koenderink, Active multistage coarsening of actin networks driven by myosin motors, Proc. Natl. Acad. Sci. U.S.A. 108 (2011) 9408–9413.
[23] D.V. Köster, K. Husain, E. Iljazi, A. Bhat, P. Bieling, R.D. Mullins, M. Rao, S. Mayor, Actomyosin dynamics drive local membrane component organization in an in vitro active composite layer, Proc. Natl. Acad. Sci. U.S.A. 113 (2016) E1645–E1654.
[24] I. Linsmeier, S. Banerjee, P.W. Oakes, W. Jung, T. Kim, M.P. Murrell, Disordered actomyosin networks are sufficient to produce cooperative and telescopic contractility, Nat. Commun. 7 (2016) 12615.
[25] M.P. Murrell, M.L. Gardel, F-actin buckling coordinates contractility and severing in a biomimetic actomyosin cortex, Proc. Natl. Acad. Sci. U.S.A. 109 (2012) 20820–20825.

[26] S. Walcott, S.X. Sun, A mechanical model of actin stress fiber formation and substrate elasticity sensing in adherent cells, Proc. Natl. Acad. Sci. U.S.A. 107 (2010) 7757–7762.
[27] E. Moeendarbary, L. Valon, M. Fritzsche, A.R. Harris, D.A. Moulding, A.J. Thrasher, E. Stride, L. Mahadevan, G.T. Charras, The cytoplasm of living cells behaves as a poroelastic material, Nat. Mater. 12 (2013) 253–261.
[28] K. Keren, P.T. Yam, A. Kinkhabwala, A. Mogilner, J.A. Theriot, Intracellular fluid flow in rapidly moving cells, Nat. Cell Biol. 11 (2009) 1219–1224.
[29] D. Zicha, I.M. Dobbie, M.R. Holt, J. Monypenny, D.Y.H. Soong, C. Gray, G.A. Dunn, Rapid actin transport during cell protrusion, Science 300 (2003) 142–145.
[30] R. Levayer, T. Lecuit, Biomechanical regulation of contractility: spatial control and dynamics, Trends Cell Biol. 22 (2012) 61–81.
[31] F.G. Woodhouse, R.E. Goldstein, Cytoplasmic streaming in plant cells emerges naturally by microfilament self-organization, Proc. Natl. Acad. Sci. U.S.A. 110 (2013) 14132–14137.
[32] M. Radszuweit, S. Alonso, H. Engel, M. Bär, Intracellular mechanochemical waves in an active poroelastic model, Phys. Rev. Lett. 110 (2013) 138102.
[33] S.W. Schneider, S. Nuschele, A. Wixforth, C. Gorzelanny, A. Alexander-Katz, R.R. Netz, M.F. Schneider, Shear-induced unfolding triggers adhesion of von Willebrand factor fibers, Proc. Natl. Acad. Sci. U.S.A. 104 (2007) 7899–7903.
[34] J. Borejdo, A. Muhlrad, S.J. Leibovich, A. Oplatka, Polymerization of G-actin by hydrodynamic shear stresses, Biochim. Biophys. Acta 667 (1981) 118–131.
[35] M. Harasim, B. Wunderlich, O. Peleg, M. Kroger, A.R. Bausch, Direct observation of the dynamics of semiflexible polymers in shear flow, Phys. Rev. Lett. 110 (2013) 108302.
[36] J.M. Ferrer, H. Lee, J. Chen, B. Pelz, F. Nakamura, R.D. Kamm, M.J. Lang, Measuring molecular rupture forces between single actin filaments and actin-binding proteins, Proc. Natl. Acad. Sci. U.S.A. 105 (2008) 9221–9226.
[37] O. Pelletier, E. Pokidysheva, L.S. Hirst, N. Bouxsein, Y. Li, C.R. Safinya, Structure of Actin cross-linked with α-actinin: a network of bundles, Phys. Rev. Lett. 91 (2003) 148102.
[38] K.M. Schmoller, O. Lieleg, A.R. Bausch, Structural and viscoelastic properties of actin/filamin networks: cross-linked versus bundled networks, Biophys. J. 97 (2009) 83–89.
[39] X. Ding, P. Li, S.-C.S. Lin, Z.S. Stratton, N. Nama, F. Guo, D. Slotcavage, X. Mao, J. Shi, F. Costanzo, T.J. Huang, Surface acoustic wave microfluidics, Lab Chip 13 (2013) 3626–3649.
[40] R.P. Hodgson, M. Tan, L. Yeo, J. Friend, Transmitting high power rf acoustic radiation via fluid couplants into superstrates for microfluidics, Appl. Phys. Lett. 94 (2009) 024102.
[41] F. Nakamura, T.M. Osborn, C.A. Hartemink, J.H. Hartwig, T.P. Stossel, Structural basis of filamin A functions, J. Cell Biol. 179 (2007) 1011–1025.
[42] T.D. Pollard, L. Blanchoin, R.D. Mullins, Molecular mechanisms controlling actin filament dynamics in nonmuscle cells, Ann. Rev. Biophys. Biomol. Struct. 29 (2000) 545–576.
[43] A. Mogilner, G. Oster, Cell motility driven by actin polymerization, Biophys. J. 71 (1996) 3030–3045.
[44] T. Kiuchi, T. Nagai, K. Ohashi, K. Mizuno, Measurements of spatiotemporal changes in G-actin concentration reveal its effect on stimulus-induced actin assembly and lamellipodium extension, J. Cell Biol. 193 (2011) 365–380.
[45] L. Blanchoin, R. Boujemaa-Paterski, C. Sykes, J. Plastino, Actin dynamics, architecture, and mechanics in cell motility, Physiol. Rev. 94 (2014) 235–263.
[46] T.D. Pollard, Actin and actin-binding proteins, Cold Spring Harbor perspectives in biology, 2016, a018226.
[47] C.P. Ng, M.A. Swartz, Mechanisms of interstitial flow-induced remodeling of fibroblast-collagen cultures, Ann. Biomed. Eng. 34 (2006) 446–454.
[48] M.D. Abràmoff, P.J. Magalhães, S.J. Ram, Image processing with imageJ, Biophotonics Intern. 11 (2004) 36–42.
[49] B. O'Connell, Oval Profile Plot. 2002.
[50] H. Nakao, M. Gad, S. Sugiyama, K. Otobe, T. Ohtani, Transfer-printing of highly aligned DNA nanowires, J. Am. Chem. Soc. 125 (2003) 7162–7163.
[51] T.T. Falzone, M. Lenz, D.R. Kovar, M.L. Gardel, Assembly kinetics determine the architecture of α-actinin crosslinked F-actin networks, Nat. Commun. 3 (2012) 861.
[52] G. Foffano, N. Levernier, M. Lenz, The dynamics of filament assembly define cytoskeletal network morphology, Nat. Commun. 7 (2016) 13827.
[53] A. Shomar, L. Geyrhofer, N.E. Ziv, N. Brenner, Cooperative stochastic binding and unbinding explain synaptic size dynamics and statistics, PLoS Comput. Biol. 13 (2017) e1005668.
[54] G. Li, J.X. Tang, Diffusion of actin filaments within a thin layer between two walls, Phys. Rev. E 69 (2004) 061921.
[55] A.J. Hunt, F. Gittes, J. Howard, The force exerted by a single kinesin molecule against a viscous load, Biophys. J. 67 (1994) 766–781.
[56] A. Kharazmi, N.V. Priezjev, Molecular dynamics simulations of the rotational and translational diffusion of a Janus rod-shaped nanoparticle, J. Phys. Chem. B 121 (2017) 7133–7139.
[57] E. Furlani, K. Ng, Analytical model of magnetic nanoparticle transport and capture in the microvasculature, Phys. Rev. E 73 (2006) 061919.
[58] B.R. Daniels, B.C. Masi, D. Wirtz, Probing single-cell micromechanics in vivo: the microrheology of C. elegans developing embryos, Biophys. J. 90 (2006) 4712–4719.
[59] W.A. Shelton, K.D. Bonin, T.G. Walker, Nonlinear motion of optically torqued nanorods, Phys. Rev. E 71 (2005) 036204.
[60] T. Kim, W. Hwang, R.D. Kamm, Computational analysis of a cross-linked actin-like network, Exp. Mech. 49 (2009) 91–104.
[61] T. Kim, M.L. Gardel, E. Munro, Determinants of fluidlike behavior and effective viscosity in cross-linked actin networks, Biophys. J. 106 (2014) 526–534.
[62] C. Borau, T. Kim, T. Bidone, J.M. García-Aznar, R.D. Kamm, Dynamic mechanisms of cell rigidity sensing: insights from a computational model of actomyosin networks, PLoS One 7 (2012) e49174.
[63] T. Shimmen, E. Yokota, Cytoplasmic streaming in plants, Curr. Opin. Cell Biol. 16 (2004) 68–72.
[64] O.L. Lewis, S. Zhang, R.D. Guy, J.C. del Álamo, Coordination of contractility, adhesion and flow in migrating Physarum amoebae, J. R. Soc. Interface 12 (2015) 20141359.
[65] K. Matsumoto, S. Takagi, T. Nakagaki, Locomotive mechanism of physarum plasmodia based on spatiotemporal analysis of protoplasmic streaming, Biophys. J. 94 (2008) 2492–2504.
[66] M.A. Choma, A.K. Ellerbee, S. Yazdanfar, J.A. Izatt, Doppler flow imaging of cytoplasmic streaming using spectral domain phase microscopy, J. Biomed. Opt. 11 (2006) 024014.
[67] J.H. Shin, M.L. Gardel, L. Mahadevan, P. Matsudaira, D.A. Weitz, Relating microstructure to rheology of a bundled and cross-linked F-actin network in vitro, Proc. Natl. Acad. Sci. U.S.A. 101 (2004) 9636–9641.
[68] H. Lee, J.M. Ferrer, F. Nakamura, M.J. Lang, R.D. Kamm, Passive and active microrheology for cross-linked F-actin networks in vitro, Acta. Biomater. 6 (2010) 1207–1218.
[69] M.M.A.E. Claessens, C. Semmrich, L. Ramos, A.R. Bausch, Helical twist controls the thickness of F-actin bundles, Proc. Natl. Acad. Sci. U.S.A. 105 (2008) 8819–8822.
[70] E.F. Koslover, C.K. Chan, J.A. Theriot, Cytoplasmic flow and mixing due to deformation of motile cells, Biophys. J. 113 (2017) 2077–2087.
[71] J.S. Lee, P. Panorchan, C.M. Hale, S.B. Khatau, T.P. Kole, Y. Tseng, D. Wirtz, Ballistic intracellular nanorheology reveals ROCK-hard cytoplasmic stiffening response to fluid flow, J. Cell. Sci. 119 (2006) 1760–1768.
[72] T.P. Kole, Y. Tseng, L. Huang, J.L. Katz, D. Wirtz, Rho kinase regulates the intracellular micromechanical response of adherent cells to rho activation, Mol. Biol. Cell 15 (2004) 3475–3484.
[73] R. Niwayama, H. Nagao, T.S. Kitajima, L. Hufnagel, K. Shinohara, T. Higuchi, T. Ishikawa, A. Kimura, Bayesian inference of forces causing cytoplasmic streaming in Caenorhabditis elegans embryos and mouse oocytes, PLoS One 11 (2016) e0159917.
[74] R.A. Lindner, G.B. Ralston, Macromolecular crowding: effects on actin polymerisation, Biophys. Chem. 66 (1997) 57–66.
[75] I.A. Gagarskaia, O.I. Povarova, V.N. Uversky, I.M. Kuznetsova, K.K. Turoverov, The effects of crowding agents Dextran-70k and PEG-8k on actin structure and unfolding reaction, J. Mol. Struct. 1140 (2017) 46–51.
[76] B. Huber, M. Harasim, B. Wunderlich, M. Kroger, A.R. Bausch, Microscopic origin of the non-newtonian viscosity of semiflexible polymer solutions in the semidilute regime, ACS Macro Lett. 3 (2014) 136–140.
[77] J.H. Hartwig, P. Shevlin, The architecture of actin filaments and the ultrastructural location of actin-binding protein in the periphery of lung macrophages, J. Cell Biol. 103 (1986) 1007–1020.
[78] J.L. Podolski, T.L. Steck, Length distribution of F-actin in Dictyostelium discoideum, J. Biol. Chem. 265 (1990) 1312–1318.
[79] F. Gittes, B. Mickey, J. Nettleton, J. Howard, Flexural rigidity of microtubules and actin filaments measured from thermal fluctuations in shape, J. Cell Biol. 120 (1993) 923–934.
[80] G.I. Bell, Models for the specific adhesion of cells to cells, Science 200 (1978) 618–627.
[81] H. Lee, B. Pelz, J.M. Ferrer, T. Kim, M.J. Lang, R.D. Kamm, Cytoskeletal deformation at high strains and the role of cross-link unfolding or unbinding, Cell. Mol. Bioeng. 2 (2009) 28–38.
[82] A.J. Ehrlicher, F. Nakamura, J. Hartwig, D. Weitz, T. Stossel, Mechanical strain in actin networks regulates FilGAP and integrin binding to filamin A, Nature 478 (2011) 260–263.
[83] H. Lee, J.M. Ferrer, M.J. Lang, R.D. Kamm, Molecular origin of strain softening in cross-linked F-actin networks, Phys. Rev. E 82 (2010) 011919.
[84] T. Kim, W. Hwang, H. Lee, R.D. Kamm, Computational analysis of viscoelastic properties of crosslinked actin networks, PLoS Comput. Biol. 5 (2009) e1000439.
[85] S. Nawaz, P. Sánchez, K. Bodensiek, S. Li, M. Simons, I.A. Schaap, Cell visco-elasticity measured with AFM and optical trapping at sub-micrometer deformations, PLoS One 7 (2012) e45297.
[86] S. Boeynaems, S. Alberti, N.L. Fawzi, T. Mittag, M. Polymenidou, F. Rousseau, J. Schymkowitz, J. Shorter, B. Wolozin, L. Van Den Bosch, Protein phase separation: a new phase in cell biology, Trends Cell Biol. 28 (2018) 420–435.
[87] P. Valberg, H.A. Feldman, Magnetic particle motions within living cells. Measurement of cytoplasmic viscosity and motile activity, Biophys. J. 52 (1987) 551–561.
[88] G.G. Borisy, T.M. Svitkina, Actin machinery: pushing the envelope, Curr. Opin. Cell Biol. 12 (2000) 104–112.
[89] H. Yin, J. Hartwig, The structure of the macrophage actin skeleton, J. Cell Sci. Suppl. 9 (1988) 169–184.
[90] L. Blanchoin, K.J. Amann, H.N. Higgs, J.-B. Marchand, D.A. Kaiser, T.D. Pollard, Direct observation of dendritic actin filament networks nucleated by Arp2/3 complex and WASP/Scar proteins, Nature 404 (2000) 1007–1011.
[91] J.T. Parsons, A.R. Horwitz, M.A. Schwartz, Cell adhesion: integrating cytoskeletal dynamics and cellular tension, Nat. Rev. Mol. Cell Biol. 11 (2010) 633–643.